Fragmentation of gold projectiles with energies of 200–980 MeV/nucleon. I. Experimental method, charge yields, and transverse momenta

J. Dreute, W. Heinrich, G. Rusch, and B. Wiegel
Fachbereich Physik, Universität GH Siegen, 5900 Siegen, Germany
(Received 21 February 1991)

A stack containing plastic nuclear track detectors and Ag target foils was exposed to a ^{197}Au beam with an energy of 980 MeV/nucleon. The analysis was restricted to energies between beam energy and 200 MeV/nucleon. 2496 collisions with Ag target nuclei and 4114 with the lighter constituents H, C, and O of the detector material were analyzed in detail. For all interactions, projectile fragments with charge $Z_F \geq 6$ were measured and their emission angles were determined. This paper describes the experiment and presents charge yields and results about transverse momenta for events with different multiplicities. Details of multiplicity distributions, correlations between fragments and signatures related to multifragmentation as a critical process are discussed in a separate paper.

I. INTRODUCTION

Since Berkeley BEVALAC started to operate in the seventies, nucleus-nucleus collisions at high energies have been investigated in many experiments. The main interest was to probe the properties of highly compressed nuclear matter and to extend our knowledge of the nuclear equation of state far away from equilibrium. A few years ago experiments were started at the CERN SPS (Super Proton Synchotron) and at the Brookhaven AGS (Alternating Gradient Synchotron) using ultrarelativistic nuclear projectiles to investigate signatures of the quark-gluon plasma transition. For these experiments central collisions transferring a maximum amount of energy into the colliding system are of particular interest. Various properties of particles produced in the interactions and of so-called participants, i.e., nucleons involved in the interactions were investigated. The field of spectator physics dealing with properties of larger pieces surviving the collisions attracted less attention, but several interesting phenomena were found in this region. A review article summarizing nuclear fragmentation results at relativistic energies was given by Hüfner [1].

Fragmentation of target nuclei has been investigated over several decades in proton-nucleus collisions. With the operation of relativistic heavy-ion accelerators it became possible to study projectile fragments. A wide spectrum of charges ranging from small values of Z_F up to the charge of the fragmenting nucleus is produced. Different mechanisms contribute to the breakup of the colliding nuclei. Spallation reactions in which fragments with large size are produced are the dominating process for light and medium size nuclei. Spallation cross sections decrease with increasing $\Delta Z = Z_P - Z_F$.

For interactions of heavier nuclei additional processes become important. In a peripheral collision where only a small amount of energy is transferred a heavy nucleus can undergo fission. Furthermore interactions are observed in which the deexcitation results in the production of several nuclear fragments of smaller size.

This process is called multifragmentation. Within the last few years the fragmentation of heavy systems gained interest since the question was raised whether multifragmentation is related to a phase transition of nuclear matter or whether it is only a statistical process. Charge and mass yields of fragments and their momentum distributions were investigated in several experiments. But most experiments were restricted to inclusive measurements. A more detailed understanding of the fragmentation process, especially for heavy systems, requires measuring fragments in coincidence. Only a few experiments of this type have been performed so far [2–4].

We used nuclear track detectors in combination with automatic track measurement to investigate the breakup of a heavy projectile. In this paper we describe the experimental method and present charge yields and results for transverse momenta. An introduction to the special topics will be given in the particular sections and an introduction to the problem of multifragmentation is given in Ref. [5].

II. EXPERIMENTAL TECHNIQUE

A. Plastic nuclear track detectors

Strongly ionizing particles passing through plastic detector foils form latent tracks of damaged material along their path. If the damage exceeds a threshold, the tracks can be developed by etching. The etch cones are visible through an optical microscope. Plastic nuclear track detectors have some unique characteristics in comparison to other detectors. They record the energy loss of ionizing particles with high precision. Furthermore the spatial resolution of measured particle trajectories is excellent. Exposures of these passive detectors to a particle beam are very simple. The typical beam time needed for the experiments described in this paper is only several minutes.

A disadvantage of plastic track detectors is the tremendous effort which is necessary to scan the detectors and

to measure the tracks. We have reduced this problem by developing methods for completely automated track measurements [6]. Using this experimental technique experiments with high statistical significance were performed in the field of heavy-ion fragmentation at different accelerators [7].

Projectile fragments coming out of the same interaction point and going into forward direction form separate etch cones. Since the damaged region along a particle trajectory has a width of less than 5 nm only a small transverse momentum is necessary to separate these tracks. This is important for the investigation of multifragmentation interactions with plastic nuclear track detectors.

B. Experimental setup

We exposed an experiment to a beam of 980 MeV/nucleon ^{197}Au at the Berkeley BEVALAC. The experiment was designed as a stack which contains alternating CR-39 ($C_{12}H_{18}O_7$) foils of 600 μm thickness used as target and detector and Ag target foils of 200 μm thickness. CR-39 is the most sensitive plastic nuclear track detector known. It records tracks of relativistic carbon nuclei with 100% efficiency and boron nuclei with some reduced efficiency.

All together 25242 projectiles entered the stack within an area of 7×5 cm^2 perpendicular to the detector surface. The beam particles penetrating the stack were continuously slowed down and finally stopped in the stack. The results presented in this paper include only interactions at energies between the maximum beam energy and 200 MeV/nucleon. Since the detection efficiency of fragments with charges $Z_F \leq 5$ depends on energy and is fluctuating near the threshold we have restricted the results reported here to fragments with charges $Z_F \geq 6$.

C. Automatic track measurements and corrections of the raw data

Image analysis computers can be used very efficiently if one restricts the measurement of the etch cones to the surface of the detector. The detector foils are mounted on a microscope stage which is moved by microprocessor controlled stepping motors. In direct illumination the etch cones of particle tracks with incidence perpendicular to the detector surface appear as dark circles on a bright background. They are detected completely automatically and their position in the field of view and their area that is correlated to the energy loss of the particles are measured. Scanning and measuring 30000 tracks on one foil side took 6 hours of system operation. All together, 180 foil sides were measured.

The edges of the dark etch cones are detected in the digitized video image based on a constant threshold in grey level. This is a very simple and fast procedure but it causes systematic errors of measured track areas if the illumination is not completely homogeneous. This so-called shading, which is also caused by electronic effects in the video camera tube, was corrected after measurement, as recently described by Rusch *et al.* [8]. In addition to shading effects it is also important to correct for effects of nonhomogeneous detector sensitivity. The sensitivity and the measured track area changes slightly from foil to foil and also with the position on the detector foil. Corrections for this effect are based on the mean area of etch cones measured for beam particles.

D. Reconstruction of trajectories and detection of interactions

A particle trajectory is determined by tracing the etch cones from one foil side to the next one. For that purpose the coordinates of measured etch cones have to be correlated to an absolute three-dimensional coordinate system. They are measured with a precision of a few microns relative to each other on one foil side. The coordinates of two adjacent foil sides fluctuate in the order of 100 μm due to mounting conditions in the stack. They are aligned more precisely using tracks of beam particles which are identified by their typical pattern of positions. A spatial resolution of $\sigma = 5$ μm remains for all tracks on one foil side.

Charge changing nuclear fragmentations are detected as a step in the area of the etch cones measured along a trajectory. An example is shown in Fig. 1 where a Au projectile undergoes a fragmentation behind foil side 25 of the stack. A fragment produced in this interaction shows etch cones with a smaller area due to its smaller charge of $Z=41$. This area is increasing with depth in the stack, since the energy loss of the fragment is slightly increasing. Further interactions of this fragment are observed behind foil side 88. For details see figure caption.

The efficiency to detect fragmentation interactions depends on the size of the step of the measured track area compared to their fluctuations along the trajectory. For events of that type shown in Fig. 1 it is evident that these interactions are detected with 100% efficiency. The size of the measured track area changes only slightly with charge for beamlike particles. For this reason interactions of Au projectiles with small charge changes ΔZ are

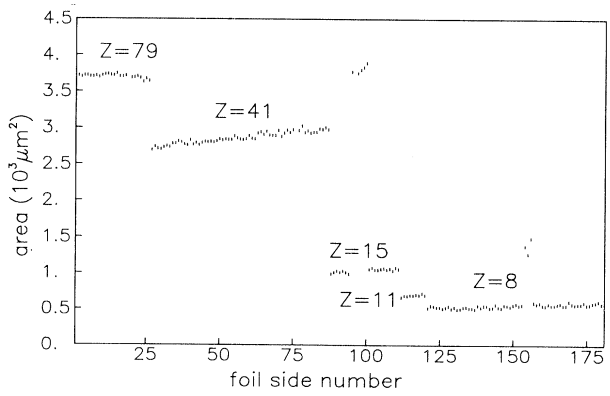

FIG. 1. Measured track areas for one incoming beam particle as a function of the stack depth. Charge-changing interactions can be observed by steps of the track area at foil sides 25, 88, 111, and 120. Around foil sides 95 and 155 the particle crosses the trajectories of other particles in the stack. At these points overlapping etch figures with significantly larger areas are measured.

not detected. Based on measurements and parametric fits for cross sections of Au in different targets by Cummings *et al.* [9,10] we estimate that about 6300 spallation interactions are missed. The detection efficiency is 100% for fission and multifragmentation interactions with fragments of charge $6 \leq Z_F \leq 60$.

E. Reconstruction of interaction vertices

In a detailed analysis of all etch cones lying within a cylinder with a diameter of 8 mm on the 10 foil sides upstream and 20 foil sides downstream of an interaction point we find almost all projectile fragments produced in this interaction. Reconstruction of interaction vertices was done interactively with programs displaying the measured data on a computer terminal. Figure 2 shows a set of fragment trajectories that were produced in a multifragmentation interaction. To ensure that all tracks visible in our detectors are included in the reconstructed interaction vertices we tried to trace additional trajectories under less strong conditions. The detected candidates were all analyzed in detail and only a few real particle trajectories were found. Thus the detection efficiency for fragments with a charge $Z_F \geq 6$ is 100% and does not depend on the multiplicity M of the event.

We took special care of tracks of particle trajectories with rapidly increasing energy loss produced in the interaction and moving only a few detector foils into forward direction. These particles, which are mainly α particles originating from the target, were eliminated from the data.

All together 6610 vertices with different fragment multiplicities were analyzed. The complete procedure of reconstruction of interaction vertices by interactive programs limits the statistics of this type of experiment. With new methods and new experimental setups that were also exposed to heavy projectiles at the BEVALAC it is possible to do the reconstruction of interaction vertices completely with computer programs. This work is under progress.

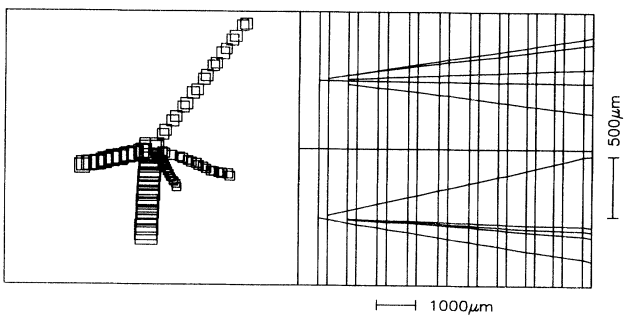

FIG. 2. Multifragmentation event with five visible fragments. The left side shows the projection into a plane perpendicular to the beam direction. The size of the squares is proportional to the track area. The right side shows the projection seen from the side and from above.

F. Detector calibration and charge resolution

The area of the etch cones is correlated to the energy loss of the particle and thus can be used to determine the charge of the particle. The etch cone is formed by two competing etching mechanisms. The surface of the detector foil is etched with the bulk etch rate v_B, whereas the damaged region of a track etches with the higher track etch rate v_T, which is a function of the restricted energy loss (REL) of the particle. It is defined as that part of the energy loss including only ionizations in which δ electrons with an energy below a threshold ω_0 are generated. For track formation in CR-39 ω_0 was determined to be $\omega_0 = 200$ eV [11].

We measure the area A of the circular mouth of the etch cones on the surface of the foil. The relation between track etch rate v_T and track area A is [12]

$$v_T = v_B[\pi(v_B t)^2 + A]/[\pi(v_B t)^2 - A] ,$$

$$\text{with } t = \text{ etching time} . \quad (1)$$

A calibration of the detector material is equivalent to determine the function $v_T = f_1(\text{REL})$ or, since $\text{REL} = f_2(Z,E)$ with charge Z and energy E, the function $Z = f(v_T,E)$. This calibration must be repeated for each experiment because it changes with each batch of plastic material and for a given batch even with time and exposure conditions.

For fragments with energies above 800 MeV/nucleon, i.e., within the first eleven detector foils of the stack the REL changes only slightly with energy. Therefore the mean areas along the trajectories of these fragments are only a function of the charge. They are presented in Fig. 3. For small areas fragments of different charge show clearly separated peaks. The charges of these fragments were identified based on a calibration of an earlier experiment using the same batch of plastic [13]. A charge $Z_F = 6$ was assigned to the second lowest peak of Fig. 3.

This charge assignment is confirmed by a comparison

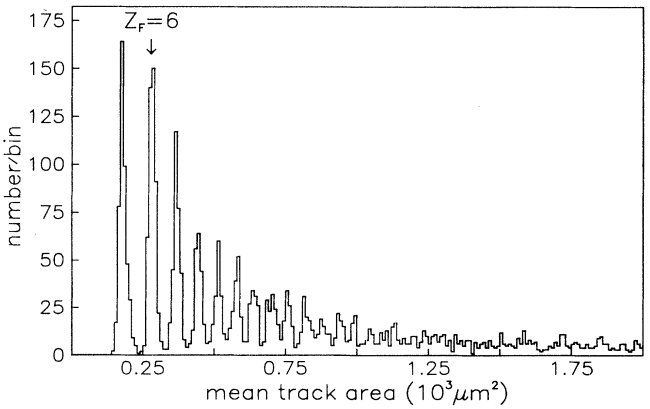

FIG. 3. Histogram of mean track areas of etch cones along the trajectory for light fragments of ^{197}Au projectiles with energies above 800 MeV/nucleon.

of charge yields of relativistic fragments measured in a new experiment presently under analysis. In this new experiment charges of fragments are unambiguously identified by counting the peaks below the beam.

The calibration curve relating v_T/v_B-1 to REL is shown in Fig. 4. The circles represent the calibration of the earlier experiment investigating the fragmentation of iron, whereas calibration points for this experiment are drawn as squares. The sequence of squares at low REL values up to about 400 MeV/(g cm^{-2}) were determined from fragments with energies above 800 MeV/nucleon as shown in Fig. 3. A lot of tracks that originate from nonfragmenting Au projectiles are available for energies between zero and maximum beam energy. From the mean area of those tracks three calibration points at very high REL were determined. The track etch rate at these high REL's saturates, resulting in a reduced charge resolution of our detector. In the region of REL between about 5×10^2 and 10^4 MeV/(g cm^{-2}) the calibration curve was drawn as a smooth curve under the condition that charge conservation for fission events is achieved. This procedure implies systematic uncertainties of charges $\Delta Z=\pm4$ assigned to fragments in this region.

Because of the stronger increasing REL at low energies the fragment charge cannot be derived from the mean track area. A typical event of this type is shown in Fig. 5. Assuming that the velocity has not changed at the point of interaction the charge that fits the measured areas best is assigned to the fragment.

Figure 6 shows a histogram of measured fragment charges with $Z_F\leq40$ and energies $E\geq200$ MeV/nucleon. The charge resolution is excellent at small charges and decreases with increasing charge. We find the charge resolution for fragments to be $\sigma(Z_F=6)=0.1e$, $\sigma(Z_F=26)=1e$ and for projectiles $\sigma(Z=79)=2e$, respectively. The fragments with charges $26\leq Z_F<79$ have an additional systematic uncertainty due to the interpolated values of the calibration curve in this range.

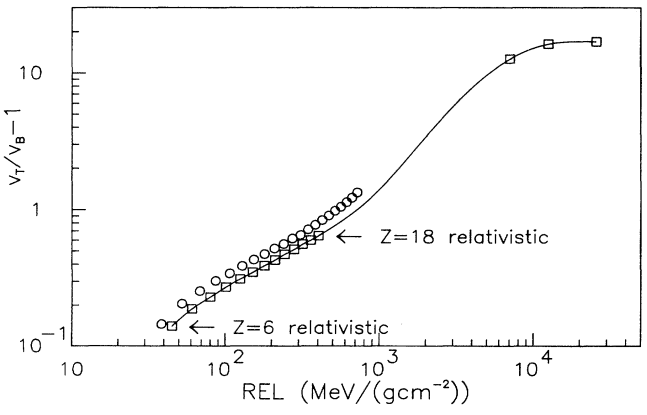

FIG. 4. Calibration curve relating v_T/v_B-1 to restricted energy loss REL. The squares are the calibration points for this experiment. The solid line shows the fitted calibration curve. The circles show the calibration of an earlier experiment using the same plastic material [11].

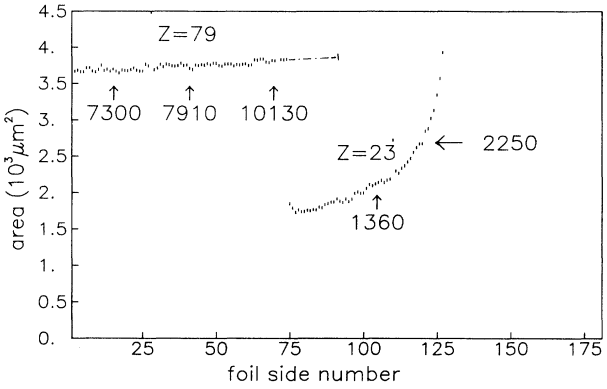

FIG. 5. Area of etch cones as the function of stack depth for a particle with an interaction at low energy. A fragment of charge $Z=23$ with an energy of 307 MeV/nucleon is produced behind foil side 74. For this fragment the measured area increases with depth since REL increases and with it v_T/v_B as shown in Fig. 4. The numbers give the REL values in MeV/(g/cm^2) at the indicated positions. The dashed line shows the mean area for a nonfragmenting projectile that is expected to stop before foil side 93.

III. CHARGE YIELDS FOR DIFFERENT MULTIPLICITIES

Figure 7 shows the yield of projectile fragments detected in our experiment separately for Ag and CR-39 target. The measured yield of spallation products is suppressed as explained above. Therefore we do not observe the expected rise of the charge yield for spallation fragments with $65\leq Z_F\leq78$. For fragments with small charges $Z_F<20$ a very high yield due to fragments produced in multifragmentation reactions is observed. Contributions of different interaction mechanisms can be studied in detail by a presentation of the charge yield for different multiplicities M. This information is presented in Fig. 8 separately for the two targets Ag and CR-39.

Contributions by deep spallation producing fragments with charges $30\leq Z_F\leq60$ are significant for $M=1$

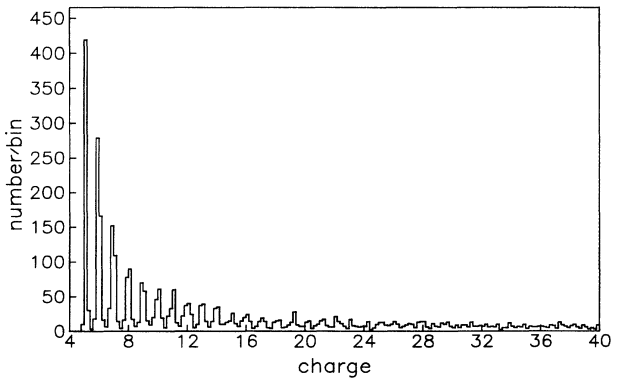

FIG. 6. Histogram of measured charges for light projectile fragments.

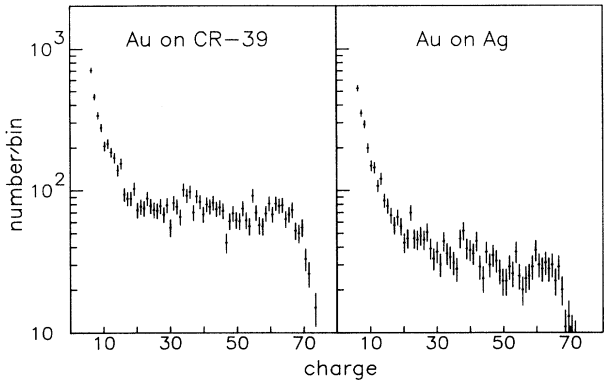

FIG. 7. Charge distribution of all observed fragments for energies between 200 and 980 MeV/nucleon, separately for the two targets.

events. They are more abundant in collisions with the light constituents of the CR-39 target ($C_{12}H_{18}O_7$). An increased yield of light fragments with $Z_F \leq 20$ is observed especially for the Ag target. These events are assumed to originate from multifragmentation interactions in which we only see the heaviest of several light fragments due to our detection threshold of $Z_F \geq 6$.

Multifragmentation events with two light fragments visible in our detectors dominate the yield for $M=2$ interactions. Contributions by fragments with a charge around $Z_F=40$ that are attributed to fission are significant. They are more abundant for interactions with the CR-39 target than with the Ag target. The yield of fragments falls for charges above half the projectile charge. These particles are produced in events with typically one light and one heavy fragment. Since the sum of their charges is significantly below the charge of the projectile they cannot be explained by asymmetric fission. In the subsequent paper [5] in which more details of charge correlations are discussed these events are called associated spallation.

For events with $M \geq 3$ the charge yield is getting steeper with increasing multiplicity. For $M=3$ we observe contributions by events with two small charges and one significantly larger charge. The yield of light fragments can be described by an exponential function that would show straight lines in Fig. 8. Deviations from this exponential function in the form of a power law as it is predicted for critical phenomena [14] is indicated by an enlarged yield of $Z=6$ and $Z=7$ fragments in some cases. However, our data, which are restricted to fragments with $Z_F \geq 6$, cannot distinguish between a power law and an exponential yield for multifragmentation events.

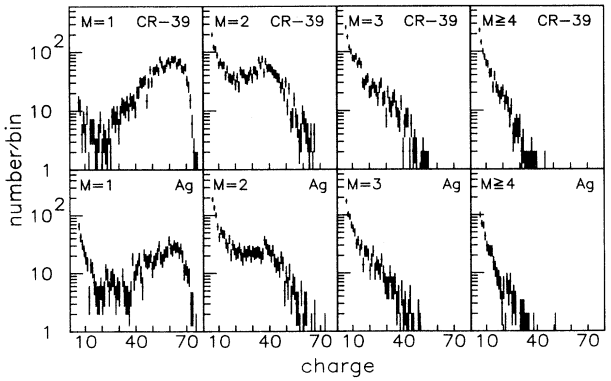

FIG. 8. Charge distribution of fragments separated for different multiplicities and for both targets.

IV. TRANSVERSE MOMENTA

Transverse momenta of fragments produced in interactions with energies above 200 MeV/nucleon were only measured in a few experiments. The distributions of the x and y components of the transverse momenta of fragments were investigated for light projectiles ^{16}O at 2.1 GeV/nucleon and ^{12}C at 1.05 and 2.1 GeV/nucleon by Greiner *et al.* [15]. These distributions can be described by Gaussians. The observed variances σ^2 show a dependence on the mass numbers of projectile P and fragment F in the form $\sigma^2=\sigma_0^2 F(P-F)/(P-1)$. This observation was explained by the statistical model of Goldhaber [16] in which the only correlation among the nucleons is given by momentum conservation. The momenta of the fragments are governed by the momentum distribution of the nucleons inside the cold projectile before the collision. For a Fermi gas of nucleons the statistical model predicts $\sigma_0^2=p_F^2/5$, with the Fermi momentum p_F of the projectile nucleus. This simple picture was remarkably successful with fitted values of σ_0 being about 10%–20% smaller than the predicted value. It also agrees in general with data of Viyogi *et al.* [17] who measured transverse momenta of fragments from Ar projectiles of 213 MeV/nucleon. Recently Gerbier *et al.* [18] have shown that the results of Greiner *et al.* hold also for ^{16}O projectiles at 200 GeV/nucleon. Considering additional details like Pauli suppression of momentum fluctuations [19], or the fact that the removed nucleons based on the peripheral nature of the fragmentation reactions have on average smaller momenta [20], or the fact that nucleons in the projectile cannot be sampled completely at random [21], reduces the values of the variances predicted by the statistical model and improves the agreement with experimental data.

However, experimental data can be explained also by a substantially different scenario. If one assumes a postcollision equilibration before breakup of the projectile the dependence of the momentum variances on projectile and fragment mass essentially have the same parabolic form like predicted from the statistical model. But under these assumptions σ_0^2 is directly proportional to the temperature of the system [16]. Temperatures of 7–9 MeV/nucleon are required to reproduce the existing data.

The experimental and theoretical situation summarized above was described in more detail in a review article by Stokstad [22]. Unpublished data of one of our earlier experiments investigating projectile fragmentation [13]

show that measured momentum variances of fragments increase in comparison to predictions of the statistical model with increasing projectile charges in the region $8 \leq Z_p \leq 26$. The only measurement of transverse momenta of heavy projectile fragments so far was performed by Brady *et al.* [23], who investigated the fragmentation of 1.2 GeV/nucleon ^{139}La nuclei in collision with carbon target. They found that momentum distributions of fragments with $26 \leq Z_F \leq 56$ are Gaussians but significantly broader than predicted by the statistical model. We will compare our results with their data.

A. Measurement of the transverse momenta

We determine the emission angles of each fragment relative to the direction of the incoming projectile from the reconstructed three-dimensional trajectories. For a fragment with mass number F emitted under azimuth angle ϑ and polar angle φ by a projectile of mass number P with a projectile momentum p_o the two components of the fragment's transverse momentum are determined by

$$\begin{pmatrix} p_x \\ p_y \end{pmatrix} = \frac{F}{P} p_o \sin\vartheta \begin{pmatrix} \cos\varphi \\ \sin\varphi \end{pmatrix} . \tag{2}$$

In the term F/P, which scales the momentum of the beam particle to the momentum of the fragment, we use the mass-to-charge ratio of the beam particle to estimate the fragment mass. Equation (2) is valid under the assumption that the fragment moves into the forward direction with the same velocity as the projectile. From measurements of Greiner *et al.* [15] it is known that fragments of ^{16}O projectiles at 2 GeV/nucleon have a mean momentum loss of 150 MeV/c measured in beam direction. We restrict our analysis of the transverse momenta to beam energies above 200 MeV/nucleon. From a Monte Carlo simulation including fluctuations of p_z described by a Gaussian with $\langle \Delta p_z \rangle = -300$ MeV/c and values of σ measured for x and y components we found that in the worst case for a small fragment ($F=15$) the measured σ are systematically enlarged by 4%.

The longitudinal momentum of the projectile nucleus at the point of interaction is determined by subtracting the calculated energy loss of the projectile in the plastic-Ag stack from the energy of the incident beam particle. In this calculation uncertainties arise from the fact that Au nuclei of the beam penetrating the stack may have lost neutrons and/or protons in peripheral collisions that were not detected. The contributions to the width of the distribution of transverse momentum components caused by these uncertainties again were investigated by a simulation calculation.

Starting with Au beam particles having a Gaussian energy spectrum with a mean energy of $E=980$ MeV/nucleon and a variance of $0.5\%E$ and considering energy loss and fragmentation we have calculated the energy spectra of beam particles and fragments with charges $Z_F \geq 67$ in each depth of our experimental setup. In this calculation fragmentation properties for Au projectiles measured by Binns *et al.* [24] were used. From the results of a Monte Carlo calculation we conclude that effects of energy spread of the particles considered as beam particles enlarge the standard deviation of the transverse momentum distribution by only 4%. This error is partially compensated by the fact that for fragmenting projectiles with reduced masses we slightly underestimate p_x and p_y. We did not correct for these two effects.

The accuracy of the measured emission angles depends on the precision of alignment of each individual detector foil side with respect to the stack coordinate system and on multiple scattering. The precision is increased by restriction to local alignments for the region around the track of interest. The influence of measurement errors of emission angles on the transverse momenta can directly be evaluated. For this purpose we took parts of trajectories of fragments containing no interaction point. They were separated into two pieces. From the angle between them the components of the equivalent transverse momenta were derived. This effect enlarges σ by 0.5%.

B. Results of transverse momenta

The distributions of the x and y components of transverse momenta analyzed in our experiment are identical within statistical accuracy. Therefore we combined both sets of data. These distributions are Gaussians except for fission reactions of the Au projectiles, so we have excluded 237 fission events ($Z_1 > 30$ and $Z_2 > 30$) from further analysis. Figure 9 shows the standard deviations σ of fitted Gaussians separately for the two targets Ag and CR-39 and for fragments produced in interactions with different multiplicities M as a function of fragment mass. Because of a lack of statistics it was necessary to compile the data of transverse momentum components for several fragment charges Z_F. The horizontal bars in Fig. 9 show the interval of corresponding fragment mass. The vertical error bars give the statistical uncertainties.

Three types of curves are shown in Fig. 9. Curve number 1 was calculated using the statistical model with a Fermi momentum of $p_F = 260$ MeV/c [25] for the Au

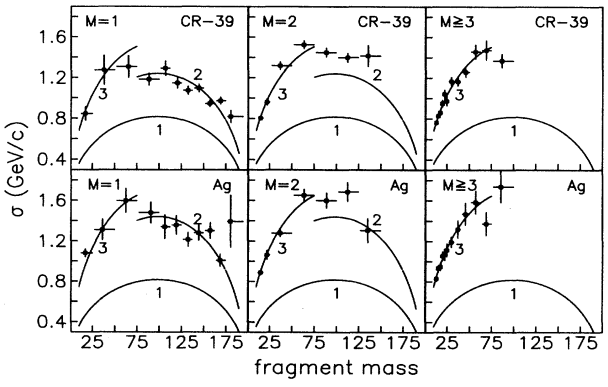

FIG. 9. The standard deviations σ of distributions of measured transverse momentum components. They are shown separately for the two targets and for different multiplicities M. The curves shown follow: curve 1, statistical model; curve 2, fit for $M=1$, $F>75$; and curve 3, fit for $M \geq 3$, $F \leq 75$.

projectile. These calculated values of σ are systematically too low. Curve number 2 is a fit to the $M=1$ data for fragment masses $F>75$ using the statistical model with σ_0 as a free parameter. Curve number 3 is a fit to the $M\geq 3$ data for fragment masses $F\leq 75$. The values of σ_0 derived by these fits are given in Table I. To investigate a possible dependence on the projectile energy we have plotted σ in Fig. 10 for different multiplicities M and for two energy regions. Values of σ_0 derived from the fitted curves are also presented in Table I.

The most significant result is that the standard deviations of transverse momentum distributions for light and heavy fragments are described by different fits. The values of σ_0 derived from the fits show that light fragments produced in multifragmentation events ($M\geq 3$) have considerably larger transverse momenta than heavy spallation events ($M=1$). Light fragments of $M=2$ and $M=1$ events show no significant deviation from curve 3, which has been fitted to $M\geq 3$ events. This supports the idea that light fragments from $M=1$ and $M=2$ interactions are multifragmentation events where the missing lighter fragments are not detected due to the experimental threshold of $Z_F\geq 6$. The standard deviations of heavy fragments from $M=2$ interactions, which are called associated spallation events [5], are enlarged in comparison to spallation events with $M=1$ (curve 2). On the other hand they are systematically smaller than the values for multifragmentation events (curve 3).

The fitted curves 2 for spallation events ($M=1, F>75$) do not fit the experimental data exactly. A statistically significant deviation with a dependence of σ_0 on the fragment mass F is indicated. For fragments with $100\leq F\leq 150$ experimentally determined values of σ show the tendency to be smaller than the fitted curve, whereas for fragments with $F>150$ the situation is vice versa. We compare these results for spallation reactions with Brady *et al.* [23]. They have fitted a value of $\sigma_0=169$ MeV/c to their data, which is consistent with our value of 176 MeV/c for the CR-39 target. Furthermore they also state that their experimental data are systematically above the fit at large F and below it at medium F.

The values of σ_0 listed in Table I show a weak dependence on the type of target material and on energy. They are larger for interactions with the Ag target than for interactions with the light nuclei H, C, and O of the CR-39 detector material. At lower energies ($E<750$ MeV/nucleon) the values of σ_0 are slightly enhanced in comparison to higher energies ($E\geq 750$ MeV/nucleon).

TABLE I. The values of σ_0 in MeV/c for curves 2 and 3 in Figs. 9 and 10.

Multiplicity M / fragment mass		1 / $F>75$	≥ 3 / $F\leq 75$
Target	Energy (MeV/nucleon)	σ_0 (MeV/c)	
CR-39	$200\leq E\leq 986$	176±3	220±2
Ag	$200\leq E\leq 986$	205±5	241±3
CR-39,Ag	$E\geq 750$	178±3	218±3
CR-39,Ag	$E<750$	189±3	236±2

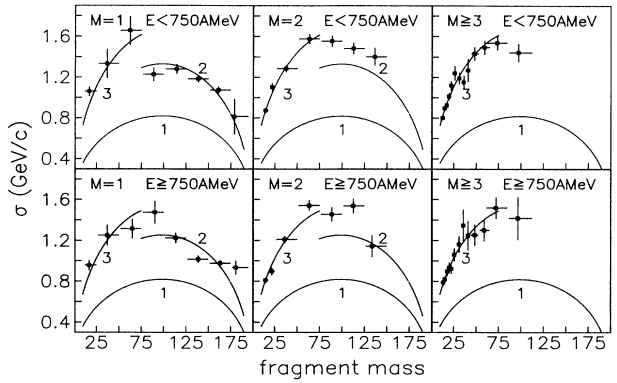

FIG. 10. The standard deviations σ of distributions of measured transverse momentum components. They are shown separately for different multiplicities M and for two energy regions. The curves shown follow: curve 1, statistical model; curve 2, fit for $M=1$, $F>75$, and curve 3, fit for $M\geq 3$, $F\leq 75$.

Details of the data presented in Fig. 9 and 10 are affected by the mass F assigned to the fragments. As already mentioned we have assumed the mass-to-charge ratio of the fragments to be the same as that of the projectile (197/79). If we use F values of stable isotopes the differences between curves 2 and 3 get smaller. If we consider the results of Cummings *et al.* [9,10] that fragments produced in spallation reactions with small ΔZ have lost a large number of neutrons the value of σ_0 for curve 2 is reduced. But the general findings from Figs. 9 and 10 mentioned above remain. A measurement of fragment masses seems to be very important; however, this is beyond our experimental technique.

The interpretation of the measured transverse momentum distributions is difficult. The statistical model describes transverse momentum distributions of fragments originating from small nuclei considerably well. It gives a lower limit for the transverse momenta because additional effects transferring momentum to the fragments are neglected. Under this point of view it is not surprising that the transverse momenta observed for heavy fragmenting systems are considerably higher than predicted by the statistical model. Several additional effects contribute to deviations from the predictions of the statistical model.

As proposed by Hüfner *et al.* [26] and by Olivera *et al.* [27] in peripheral collisions high energetic nucleons from the participant region may deposit energy inside the prefragment and thus increase its transverse momentum. Brady *et al.* [23] have explained the enlarged transverse momenta of spallation fragments based on this effect and on additional contributions by Coulomb repulsion. Our results support their idea. Especially the enlarged values of σ_0 observed for interactions with the Ag target in comparison to the light target nuclei of CR-39 and the observed energy dependence of σ_0 may indicate a more significant contribution by Coulomb repulsion.

Transverse momentum distributions of light fragments

generated in collisions of heavy projectiles with energies of several hundred MeV/nucleon have never been measured before. The standard deviations of these distributions follow the form of the fitted curve 3 quite accurately. For these fragments significant contributions which are not predicted by the statistical model lead to a broadening of the transverse momentum distributions. The fitted values of σ_0 are enhanced by a factor of more than two which may indicate a heat up of the fragmenting system before breakup. However, one has to be careful to derive temperatures from σ_0 since Coulomb repulsion and other effects certainly play an important role.

V. SUMMARY AND CONCLUSIONS

We have used a new experimental method to investigate the fragmentation of heavy projectiles exclusively for all fragments with a charge $6 \leq Z_F \leq 60$. 6610 interactions of Au projectiles were analyzed. The efficiency to detect several projectile fragments coming from the same interaction vertex is 100% and does not depend on the multiplicity M of fragments. The charge resolution for light fragments is excellent ($\sigma_{Z=6}=0.1e$). It decreases with increasing fragment charge, but is always better than $1e$ for charges $Z_F \leq 20$.

For $M=1$ a significant contribution by deep spallation events was observed. The increasing yield of light fragments for decreasing Z_F indicates a contribution by multifragmentation interactions. The $M=2$ events show contributions by associated spallation, fission, and a large yield of light fragments which we attribute to multifragmentation. With higher multiplicities the charge yield of multifragmentation fragments becomes steeper.

The measured distributions of transverse momentum components are of Gaussian shape. Variances of fitted Gaussians are significantly larger than predicted by the statistical model of Goldhaber. In general they follow the parabolic dependence on projectile and fragment mass but with different values of σ_0 for multifragmentation and spallation. The widths of the transverse momentum distributions depend also on target material and projectile energy.

ACKNOWLEDGMENTS

This work was funded by the Bundesminister für Forschung and Technologie (BMFT) under Contract No. 06 SI 146. We are grateful to the staff of the Berkeley BEVALAC for providing us with heavy-ion beams.

[1] J. Hüfner, Phys. Rep. **125**, 129 (1985).
[2] A. I. Warwick *et al.*, Phys. Rev. C **27**, 1083 (1983).
[3] C. J. Waddington and P. S. Freier, Phys. Rev. C **31**, 888 (1985).
[4] B. Jakobsson, G. Jönsson, L. Karlsson, V. Kopljar, B. Noren, K. Söderström, F. Schussler, E. Monnand, H. Nifenecken, G. Fai, J. P. Bondorf, and K. Sneppen, Nucl. Phys. **A509**, 195 (1990).
[5] C. Lewenkopf, J. Dreute, A. Abul-Magd, J. Aichelin, W. Heinrich, J. Hüfner, G. Rusch, and B. Wiegel, Phys. Rev. C **44**, 1066 (1990), the following paper.
[6] W. Trakowski, B. Schöfer, J. Dreute, S. Sonntag, C. Brechtmann, J. Beer, H. Drechsel, and W. Heinrich, Nucl. Instrum. Methods. **225**, 92 (1984).
[7] W. Heinrich, C. Brechtmann, J. Dreute, D. Weidmann, Nucl. Tracks Radiat. Meas. 15, 393 (1988); C. Brechtmann and W. Heinrich, Z. Phys. A **330**, 407 (1988); **331**, 463 (1988); C. Brechtmann, W. Heinrich, and E. V. Benton, Phys. Rev. C **39**, 2222 (1989).
[8] G. Rusch, E. Winkel, A. Noll, and W. Heinrich, in The Fifteenth International Conference on Particle Tracks in Solids, Marburg, F.R.G., 1990 [Nucl. Tracks Radiat. Meas. (in press)].
[9] J. R. Cummings, W. R. Binns, T. L. Garrad, M. H. Israel, J. Klarmann, E. C. Stone, and C. J. Waddington, Phys. Rev. C **42**, 2508 (1990).
[10] J. R. Cummings, W. R. Binns, T. L. Garrad, M. H. Israel, J. Klarmann, E. C. Stone, and C. J. Waddington, Phys. Rev. C **42**, 2530 (1990).
[11] D. L. Henshaw, N. Griffiths, O. A. L. Landen, and E. V. Benton, Nucl. Instrum. Methods **180**, 65 (1981).
[12] G. Somogyi and S. A. Szalay, Nucl. Instrum. Methods **109**, 211 (1973).
[13] H. Drechsel, C. Brechtmann, W. Heinrich, and J. Dreute, Phys. Rev. Lett. **55**, 1258 (1985).
[14] X. Campi, Phys. Lett. B **208**, 351 (1988).
[15] D. E. Greiner, P. J. Lindstrom, H. H. Heckman, B. Cork, and F. S. Bieser, Phys. Rev. Lett. **35**, 152 (1975).
[16] A. S. Goldhaber, Phys. Lett. **53B**, 306 (1974).
[17] Y. P. Viyogi, T. J. M. Symons, P. Doll, D. E. Greiner, H. H. Heckman, D. L. Hendrie, P. J. Lindstrom, J. Mahoney, D. K. Scott, K. van Bibber, G. D. Westfall, H. Wieman, H. J. Crawford, C. McParland, and C. K. Gelbke, Phys. Rev. Lett. **42**, 33 (1979).
[18] G. Gerbier, W. T. Williams, P. B. Price, and R. Guoxiao, Phys. Rev. Lett. **59**, 255 (1987).
[19] G. Bertsch, Phys. Rev. Lett. **46**, 472 (1981).
[20] W. A. Friedman, Phys. Rev. C **27**, 569 (1983).
[21] M. J. Murphy, Phys. Lett. **135B**, 25 (1984).
[22] R. G. Stokstad, Comments Nucl. Part. Phys. **13**, 231 (1984).
[23] F. P. Brady, W. B. Christie, J. L. Romero, C. E. Tull, B. McEachern, M. L. Webb, J. C. Young, H. J. Crawford, D. E. Greiner, P. J. Lindstrom, and H. Sann, Phys. Rev. Lett. **60**, 1699 (1988).
[24] W. R. Binns, T. L. Garrard, M. H. Israel, M. P. Kertzmann, J. Klarmann, E. C. Stone, and C. J. Waddington, Phys. Rev. C **36**, 1870 (1987).
[25] E. J. Moniz, I. Sick, R. R. Whitney, J. R. Ficenec, R. D. Kephart, and W. P. Trower, Phys. Rev. Lett. **26**, 445 (1971).
[26] J. Hüfner, K. Schäfer, and B. Schürmann, Phys. Rev. C **12**, 1888 (1975).
[27] L. F. Olivera, R. Donangelo, and J. O. Rasmusen, Phys. Rev. C **19**, 826 (1979).